

## Investigation of the Effect of Band Offset and Mobility of Organic/Inorganic HTM Layers on the Performance of Perovskite Solar Cells

Davoud Jalalian<sup>1</sup>, Abbas Ghadimi<sup>\*2</sup>, Azadeh Kiani Sarkaleh<sup>1</sup>

<sup>1</sup>Department of Electrical Engineering, Rasht Branch, Islamic Azad University, Rasht, Iran

<sup>2</sup>Department of Electrical Engineering, Lahijan Branch, Islamic Azad University, Rasht, Iran

(Received 28 Apr. 2020; Revised 16 May 2020; Accepted 22 May 2020; Published 15 Jun. 2020)

**Abstract:** Perovskite solar cells have become an attractive subject in the solar energy device area. During ten years of development, the energy conversion efficiency has been improved from 2.2% to more than 22%, and it still has a very good potential for further enhancement. In this paper, a numerical model of the perovskite solar cell with the structure of glass/ FTO/ TiO<sub>2</sub>/ H<sub>3</sub>NH<sub>3</sub>PbI<sub>3</sub>/ HTM/Au by using Silvaco Atlas software is presented. The effect of hole transport material characteristics, including hole mobility and band gap offset of organic and inorganic HTM layers such as Spiro-MOeTAD, CuO and Cu<sub>2</sub>O on the performance of PSCs are investigated. The simulation results reveal that with increase of hole mobility in hole transport layer, the cell efficiency is increases. Meanwhile, the solar cell exhibits a better performance by using inorganic materials like CuO and Cu<sub>2</sub>O as hole transport layer, than by using Spiro-MOeTAD, particularly the efficiency reaches 22.12% when Cu<sub>2</sub>O is used.

**Keywords:** Perovskite Solar Cell, Hole Transport Layer, HTM, Bandgap Offset, Efficiency.

### 1. INTRODUCTION

Demand for energy resources is growing with ongoing development of economy. Forecasts show that the world's population will reach 8.1 billion by 2020. This large number of populations are in great need of energy. The supply of energy required by fossil fuels is in addition to causing environmental pollution, global warming, and so on. Therefore, the need to replace clean and renewable resources today seems more urgent than ever. Photovoltaic technology

\* Corresponding author. Email: [ghadimi@liau.ac.ir](mailto:ghadimi@liau.ac.ir)

and solar cells are one of the best sources of energy. Perovskite solar cells (PSCs) have attracted much attention because of their high efficiency. However, unstable performance and expensive hole transport materials (HTM) limit its expansion. Organic materials such as Spiro-OMeTAD, PEDOT: PSS and MEH-PPV that are relatively expensive and have low mobility are used as HTM in PSCs. Some reports also confirm that the HTM layer affects cell function and a decrease in cell function has been observed with the use of organic HTM [1]. Therefore, to commercialize perovskite solar cells and dominate the photovoltaic industry, it is essential to find an alternative HTM for PSCs. Inorganic materials have been considered as suitable substitutes for organic HTM layers due to their desirable characteristics such as high mobility of holes, low fabrication cost, better chemical stability and their suitable bandgap energy [2]. Using metal oxides with p-type conductivity, superior charge carrier mobility and high stability are suitable candidates as HTMs. There are numerous reports on using p-type metal oxides including CuO, MoO<sub>3</sub>, and NiO<sub>x</sub> as HTM layer for PSCs [3-5]. Having privileged electrical and optical properties, Cu<sub>2</sub>O can be a promising candidate as HTM for PSCs. However, more studies are needed to reveal different aspects of using this material as HTM in PSCs. In the present study, by arrangement of a numerical simulation, the variation of output parameters of a PSC will be studied comparatively by considering Spiro-OMeTAD, CuO and Cu<sub>2</sub>O as HTM layer. Numerical simulation of solar cells can save time and materials needed to build and deploy them. Before proceeding with the construction, the desired structure can be designed and numerically simulated to obtain the desired output parameters and begin the laboratory work by eliminating possible defects and problems with a lower error percentage. Recently, many researchers have reported the simulation of perovskite solar cells using software such as SCAPS [6, 7], wxAMPS [8] and GPVDM [9] based on the physical model of drift and diffusion. To achieve a more objective simulated model that explains the experimental results, Silvaco Atlas [10] provides a large set of physical models of drag and drop. Various material models (organic and inorganic) have been incorporated that allow carrier recombination and mobility in order to adapt to experimental results. In this paper, a numerical simulation based on a Perovskite solar cell with Glass / FTO / TiO<sub>2</sub> / CH<sub>3</sub>NH<sub>3</sub>PbI<sub>3</sub> / HTM / Au structure is performed with the help of Silvaco Atlas software. The influence of the characteristics of the HTM layer on the performance of the Perovskite solar cell is studied here. In addition, the simulation results of two inorganic Cu<sub>2</sub>O and CuO as HTM layer options are compared to Spiro-OMeTAD, which is used as standard in PSCs.

## 2. Device structure and simulation method

The simulated perovskite solar cell configuration is shown in Fig. 1. This paper uses Silvaco Atlas simulator software which has various physical models such as

organic model for perovskite and HTM layer which are organic.  $\text{TiO}_2$  was used as electron transport layer because of very good compatibility between its conduction band and the lower unoccupied molecular orbital (LUMO) of perovskite layer. Table I presents the various materials and models used in the simulation.

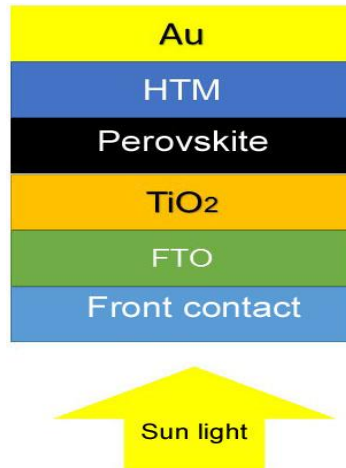


**Fig 1.** Simulated Perovskite Solar Cell Structure.

TABLE 1. The materials type and the used models to describe the carrier mobility and recombination in Silvaco Atlas.

Recombination model	Mobility model	Material type	Layer
SRH	Carrier concentration	Inorganic	ETM
And Langevin SRH	Poole-Frenkel field	Organic	HTM (Spiro-OMeTAD)
And Langevin SRH	Poole-Frenkel field	Organic	Perovskite

Table II also presents the physical properties of the materials used in the simulation, collected from various experimental works [8 and 9]. It should be noted that the Pool-Frenkel field model is suitable for the mobility of organic materials. This model is used with the Langevin recombinant model. Langevin recombination is required to enable exchange between pregnant carriers and single and ternary excitons [7]. The standard AM1.5 spectra were used in the simulation.

**TABLE II. The physical parameters for each layer used in the simulation.**

Parameters	FTO	TiO <sub>2</sub>	CH <sub>3</sub> NH <sub>3</sub> PbI <sub>3</sub>	CuO	Cu <sub>2</sub> O	Spiro-OMeTAD
Thickness (nm)	400	50	450	150	150	150
E <sub>g</sub> (eV)	3.5	3.26	1.55	1.3	2.17	2.9
χ (eV)	4	4.2	3.9	4.07	3.2	2.2
N <sub>c</sub> (cm <sup>-3</sup> )	2×10 <sup>18</sup>	2×10 <sup>18</sup>	2.2×10 <sup>18</sup>	2.2×10 <sup>18</sup>	2.2×10 <sup>18</sup>	2.2×10 <sup>18</sup>
N <sub>v</sub> (cm <sup>-3</sup> )	2×10 <sup>19</sup>	2×10 <sup>19</sup>	2.2×10 <sup>19</sup>	1.8×10 <sup>18</sup>	1.8×10 <sup>18</sup>	1.9×10 <sup>19</sup>
N <sub>D</sub> (cm <sup>-3</sup> )	10 <sup>19</sup>	10 <sup>17</sup>	10 <sup>13</sup>	-	-	-
N <sub>A</sub> (cm <sup>-3</sup> )	-	-	-	10 <sup>18</sup>	10 <sup>18</sup>	10 <sup>18</sup>
ε <sub>r</sub>	9	10	6.5	18.1	7.11	3
μ <sub>n</sub> (cm <sup>2</sup> V <sup>-1</sup> s <sup>-1</sup> )	20	20	1	0.1	80	2×10 <sup>-4</sup>
μ <sub>p</sub> (cm <sup>2</sup> V <sup>-1</sup> s <sup>-1</sup> )	10	10	1	0.1	80	2×10 <sup>-4</sup>
τ <sub>n</sub> (s)	1×10 <sup>-7</sup>	1×10 <sup>-7</sup>	1×10 <sup>-6</sup>	1×10 <sup>-7</sup>	1×10 <sup>-7</sup>	1×10 <sup>-7</sup>
τ <sub>p</sub> (s)	1×10 <sup>-7</sup>	1×10 <sup>-7</sup>	1×10 <sup>-6</sup>	1×10 <sup>-7</sup>	1×10 <sup>-7</sup>	1×10 <sup>-7</sup>

Atlas uses the following steps to calculate the output parameters of solar cells:

- 1- Specifying the solar spectra: Here, we are choosing to simulate AM1.5 conditions sampled between 0.3 microns and 1.2 microns at 50 samples:

```
BEAM NUM=1 AM1.5 WAVELENGTH.START=0.3 WAVELENGTH.END=1.2
WAVELENGTH.NUM=50
```

- 2- Solar optical propagation model: In the present study the ray tracing method was used to model the propagation of light inside the device:

```
BEAM NUM=1 AM1.5 WAVELENGTH.START=0.3 WAVELENGTH.END=1.2
WAVELENGTH.NUM=50
```

In this case, we will perform 50 ray traces.

- 3- Solar cell extraction:

(a) The first step in solar analysis is to illuminate the device. This is performed by assigning the beam intensity on a SOLVE statement as follows:

```
SOLVE B1=1.0
```

Here, we assign a value of one "sun" to the intensity of the optical source indexed as number "1" (B1).

(b) The next step is to extract the illuminated, forward current-voltage characteristic. First, we should define an output file for capturing the data. For example:

```
LOG OUTFILE="IV.LOG"
```

(c) Capture I-V characteristics:

We need to ramp the voltage past the open circuit voltage ( $V_{oc}$ ) as in the following:

```
SOLVE VANODE=0 NAME=ANODE VSTEP=0.1 VFINAL=0.5
SOLVE NAME=ANODE VSTEP=0.01 VFINAL=0.7
```

The current-voltage characteristic is observable in TonyPlot using the following:

```
TONYPLOT IV.LOG
```

4- Extracting output parameters:

We can now use the DeckBuild Extract capability to capture the various solar cell figures of merit. We **first** initialize the Extract capability with the captured input file as in the following:

```
EXTRACT INIT INFILE="IV.LOG"
```

The following lines demonstrate the extraction of short circuit current ( $I_{sc}$ ), open circuit voltage ( $V_{oc}$ ), maximum power ( $P_m$ ), voltage at maximum power ( $V_m$ ), current at maximum power ( $I_m$ ), and fill factor (FF).

```
EXTRACT NAME="Isc" Y.VAL FROM CURVE (V."anode",
I."cathode") WHERE X.VAL=0.0
```

```
EXTRACT NAME="Voc" X.VAL FROM CURVE (V."anode",
I."cathode") WHERE Y.VAL=0.0
```

```
EXTRACT NAME="Pm" MAX (CURVE (V."anode", (V."anode"
I."cathode")))
```

```
EXTRACT NAME="Vm" X.VAL FROM CURVE (V."anode",
(V."anode"*I."cathode")) \
```

```
WHERE Y.VAL=$"Pm"
```

```
EXTRACT NAME="Im" $"Pm"/$"Vm"
```

```
EXTRACT NAME="FF" $"Pm"/($"Jsc"*$"Voc")
```

Given that we know the area of the device in square cm, we can assign it to a variable and extract power efficiency as follows:

```
SET area=1e4
```

```
EXTRACT NAME="OPT_INT" MAX(BEAM."1")
```

```
EXTRACT NAME="POWER_EFF"
```

```
(ABS($"Pm")/($OPT_INT*$area))
```

To consider the probable emerging states stemming from mismatch between the absorber layer and the buffer layer, a thin layer (10 nm) named ordered vacancy compound (OVC) was considered in Perovskite/TiO<sub>2</sub> junction. The most reliable result was achieved for  $E_g=1.45$  eV,  $N_D=10^{13}$  cm<sup>-3</sup>, and  $N_c=N_v=2\times 10^{18}$  cm<sup>-3</sup> for OVC layer.

### 3. Results and discussion

#### 3.1. Impact of HTM layer attributes

We investigate the effect of hole transport material characteristics on device performance based on Spiro-OMeTAD, which is widely used in current solar cells. Hole mobility and bandgap offset are two important parameters that should be considered as criteria for selection for hole transport materials.

Figure 2 shows the results of the calculations performed on the short circuit current density (Jsc), open circuit voltage (Voc), fill factor (FF) and conversion efficiency ( $\eta$ ) in terms of hole mobility.

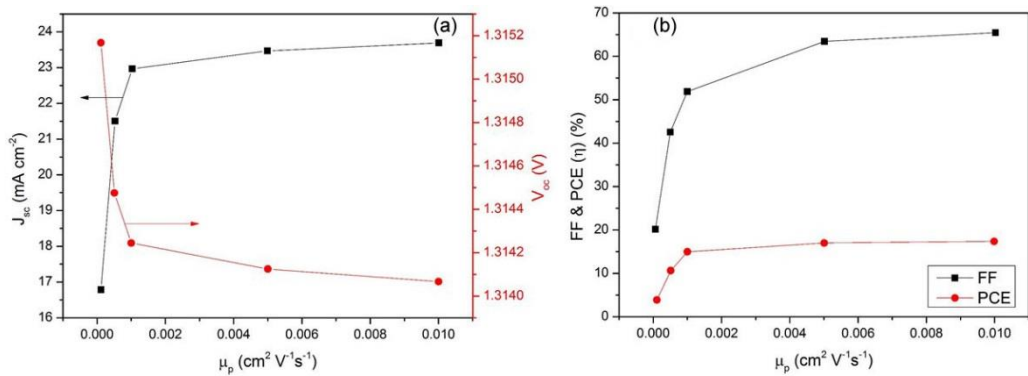


**Fig 2.** Simulated PSC performance in terms of cavity hole mobility: (a) short-circuit current and open-circuit voltage changes, and (b) FF and efficiency coefficients.

As can be seen from Fig. 2, with the exception of  $V_{oc}$ , the other device output parameters increase with increasing hole mobility. This behavior can be explained according to the following equation [13]:

$$qV_{oc} = E_g - \Delta \quad (1)$$

where

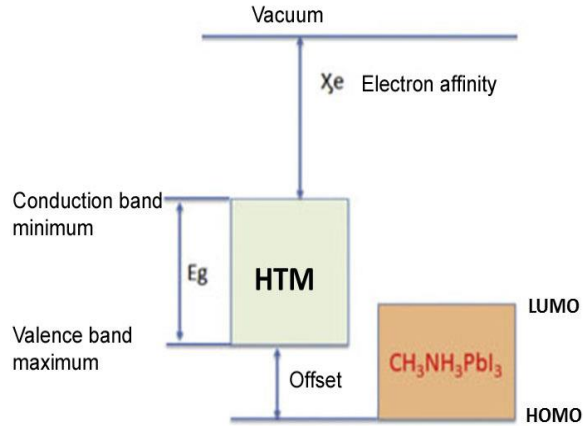
$$\Delta = 2(E_{F,h} - E_{HOMO}^D) - k_B T \ln\left(\frac{\mu_n}{\mu_p}\right) \quad (2)$$

Here  $\Delta$  is the energy loss contributed by the energetic (first term) and charge transport (second term),  $E_{F,h}$  is the energy of the hole quasi-Fermi level,  $E_D^{HOMO}$  is the energy of the donor high-occupied-molecular-orbital (HOMO),  $k_B$  is the Boltzmann constant and  $T$  denotes the absolute temperature. As can be seen from Eqs. 1 and 2,  $V_{oc}$  depends on the electron and hole mobilities directly. The material with  $\mu_n < \mu_p$  will have greater energy loss  $\Delta$  and hence lower  $V_{oc}$  in comparison with materials with  $\mu_n > \mu_p$  which will have lesser  $\Delta$  and hence higher  $V_{oc}$ . So, when the hole mobility increased (Fig. 2) and the ratio  $\mu_n / \mu_p < 1$ , the energy loss  $\Delta$  increased and resulted in reduction of  $V_{oc}$ .

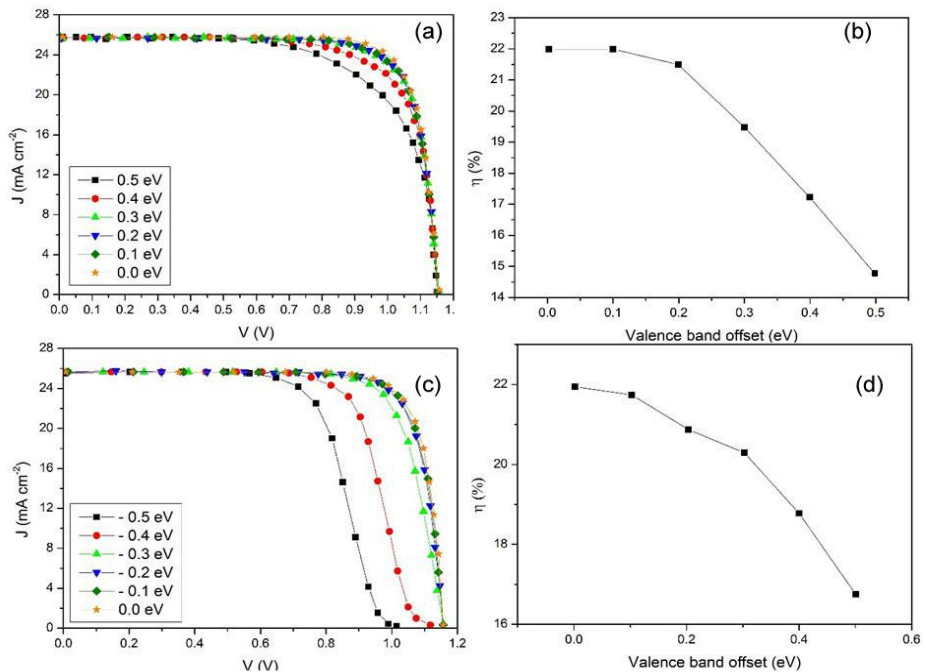
When the hole mobility reaches  $5 \times 10^{-3} \text{ cm}^2 \text{ V}^{-1} \text{ s}^{-1}$ , the  $J_{sc}$ ,  $V_{oc}$ , FF, and PCE tend to be constant. However,  $J_{sc} \sim 23 \text{ mA} \cdot \text{cm}^{-2}$ ,  $V_{oc} = 1.31 \text{ V}$ , FF=65%, and PCE is close to 17%. The high mobility of the hole leads to improved conductivity and performance of the device. Spiro-OMeTAD hole mobility is low, which is not suitable for cell function, and therefore p-type HTM layer doping is necessary to increase the motility. Thus, materials with high mobility of the hole for the hole transport layer should be considered.

As we know, the HTM layer is used to transport holes from the perovskite absorber layer while simultaneously blocking the backflow from the perovskite to the HTM, so proper location of the conduction band is crucial in the design of the device. We examine the effect of the conduction band offset on cell function in this section. A schematic view of the position of the band offset at the junction of the HTM layer and the perovskite layer is shown in Fig. 3. Different values of bandgap offset can be obtained by changing the electron affinity  $\chi$ . Both positive and negative offset values of the valence band were varied with 0.1 eV step from 0.1 to 0.5 eV. The simulation results are shown in Fig. 4. Figure 4 (a) shows the simulation results for different positive values of the valence band offset. In this case, the maximum of the valence band of HTM layer is lower than the HOMO layer of the perovskite layer. As the offset potential increases, higher potential barriers appear between the two layers. This means that the holes produced in the perovskite layer can hardly enter the HTM layer. It is also seen that as the short-circuit current and open-circuit voltage remain almost unchanged with increase in offset while the FF and, as a consequence, the efficiency decreases. The simulated cell efficiency changes in terms of offset potential are shown in Fig. 4

(b), which is expected to decrease with increasing band offset. In addition, the decrease in solar cell efficiency at offset voltages is more than 0.2 eV.



**Fig 3.** Schematic view of valence band offset at junction of HTM layer and perovskite.



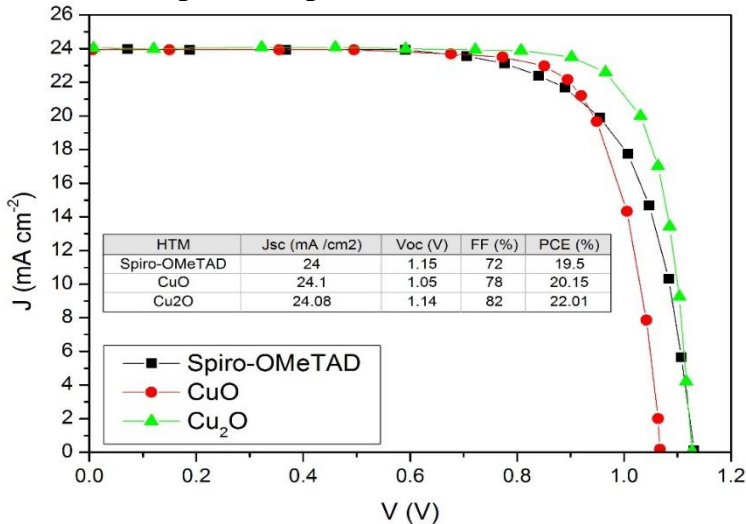
**Fig 4.** Changes in (a) current-voltage characteristic for positive offset potential values, (b) cell efficiency in terms of positive offset potential, (c) current-voltage characteristic for negative offset potential values, and (d) cell efficiency in negative offset potential.

Figure 4 (c) shows the simulation results of the current-voltage characteristic for different values of negative offset potential. In this case, the location of the HTM layer valence band is higher than the perovskite layer. The results show that the short-circuit current remains constant with the offset potential variation while the negative offset voltage increases as the open circuit voltage decreases. This reduces the cell efficiency by increasing the offset potential. The reason for this can be attributed to the difficulty in extracting the holes produced in the perovskite layer by negative offset.

### 3.2. Effect of HTM Layer Type Selection

CuO and Cu<sub>2</sub>O are p-type semiconductors and both have relatively wide bandgaps. Their bandgap values are 1.3 eV and 2.17 eV, respectively [3]. We conclude from the previous section that in order to reduce the energy loss and obtain high-performance cells, the offset between the valence band of the HTM layer and the perovskite layer must be low. The offset potential of CuO and Cu<sub>2</sub>O and perovskite layer is lower than 0.1 eV. In addition, Cu<sub>2</sub>O has a hole mobility above 80 cm<sup>2</sup>V<sup>-1</sup>s<sup>-1</sup> and CuO has a relatively high value of 0.1 cm<sup>2</sup>V<sup>-1</sup>s<sup>-1</sup> compared to Spiro-OMeTad (0.002 cm<sup>2</sup>V<sup>-1</sup>s<sup>-1</sup>). For these reasons, CuO and Cu<sub>2</sub>O are thought to be potential substitutes for HTM in perovskite solar cells.

In this section we perform simulations for three HTM layers (Spiro-OMeTAD, CuO and Cu<sub>2</sub>O) and compare the results. The results of the simulations are shown in Figure 5 and the table given in Figure.



**Fig 5.** J-V characteristic curve and output parameters table related to simulation of the effect of applying organic and inorganic HTM layers on perovskite solar cell performance.

The results show that the use of CuO and Cu<sub>2</sub>O leads to better results than the Spiro-OMeTAD. Especially for Cu<sub>2</sub>O where the efficiency reached 22.12%. Also, due to its good bandwidth, valence band position and high hole mobility, the results of its short circuit current and its open circuit voltage show high values compared to other counterparts. To better understand of the cell performance with different HTM layers, the electric field profile (corresponding to the potential) was calculated and shown in Fig. 6.

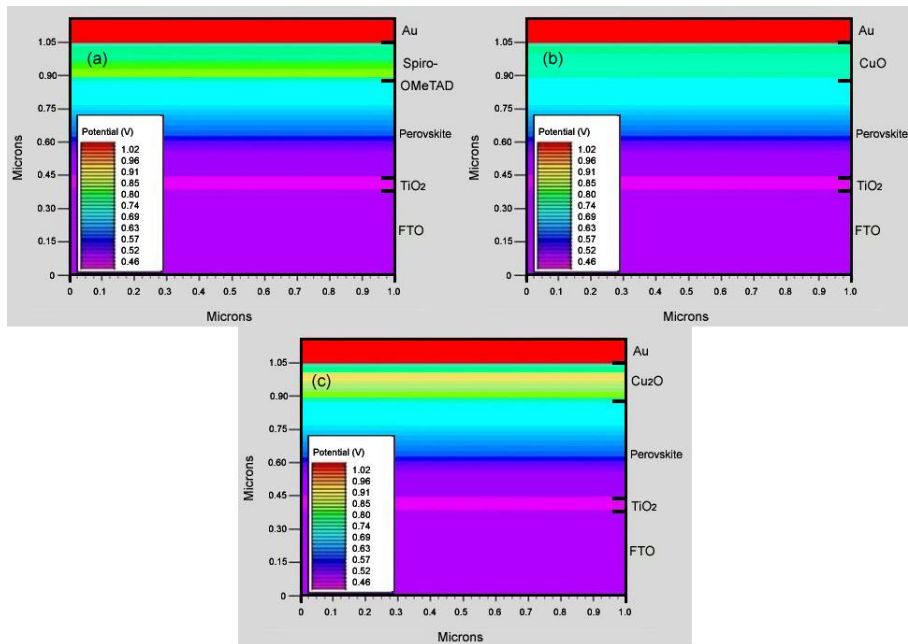


**Fig. 6.** Electric field profile for PSC with (a) Spiro-OMeTAD, (b) CuO and (c) Cu<sub>2</sub>O as the HTM layer.

The main difference between the electric field distribution profiles in Fig. 6 is the variation of electric field intensity in HTM layer. As can be seen, the background of field for Cu<sub>2</sub>O layer contains colors indicating higher intensity than that of the other counterparts. Meanwhile, it can be seen from the figure that the potential for FTO and Au is ~0.45 V and 1.02 V, respectively. This potential difference between electrodes provides a driving force for photo-generated excitons to be separated as charge carriers (electrons and holes). The existence of HTM layer with more positive potential in the vicinity of Au electrode can enforce the driving force. This can increase the built-in electric field followed by increase in  $V_{oc}$ . Such a behavior is observed in this study. Consequently, the

efficiency of solar cell may increase.

The results of this simulation illustrate the fact that CuO and Cu<sub>2</sub>O, as inorganic and relatively inexpensive compounds, are very good substitutes for the expensive Spiro-OMeTAD organic material.

#### 4. CONCLUSION

In this paper, a Perovskite solar cell with glass / FTO / TiO<sub>2</sub> / CH<sub>3</sub>NH<sub>3</sub>PbI<sub>3</sub> / HTM / Au configuration was designed and simulated using the Silvaco Atlas device simulator software. The influence of the characteristics of the HTM layer including hole mobility and valence band offset on the designed cell performance was investigated. The device performance was also studied by changing the HTM layer from Spiro-OMeTAD to CuO and Cu<sub>2</sub>O. The simulation results showed that the high mobility of the HTM layer leads to superior cell performance. For Spiro-OMeTAD, when the mobility reached  $5 \times 10^{-3} \text{ cm}^2 \text{ V}^{-1} \text{ s}^{-1}$ , the efficiency reached its maximum value, and its changes stopped after that amount with increasing mobility. The valence band offset showed a profound effect on the cell functionality. Both positive and negative band offset had a significant effect on the cell performance. The results revealed that the band offset between -0.2 eV and +0.2 eV resulted in the best device performance. Finally, by considering the optimum values and also using Cu<sub>2</sub>O as HTM, the 22.2% optimum efficiency was achieved for the solar cell.

#### REFERENCES

- [1] A. K. Jena, Y. Numata, M. Ikegami, T. Miyasaka, *Role of spiro-OMeTAD in performance deterioration of perovskite solar cells at high temperature and reuse of the perovskite films to avoid Pb-waste*. J. Mater. Chem. A, 6 (2018, Winter) 2219-2230.  
Available: <https://pubs.rsc.org/en/content/articlelanding/2018/ta/c7ta07674f#!divAbstract>
- [2] C. Tseng, L. Chen, L. Chang, G. Wu, W. Feng, M. Jeng, D. W. Chen, K. Lee, *Cu<sub>2</sub>O-HTM/SiO<sub>2</sub>-ETM assisted for synthesis engineering improving efficiency and stability with heterojunction planar perovskite thin-film solar cells*, Sol. Energy, 204 (2020, Summer) 270-279.  
Available: <https://www.sciencedirect.com/science/article/pii/S0038092X20304618>
- [3] X. Miao, S. Wang, W. Sun, Y. Zhu, C. Du, R. Ma, C. Wang. *Room-temperature electrochemical deposition of ultrathin CuOx flm as hole transport layer for perovskite solar cells*. Scr. Mater. 165 (2019, Spring) 134-9.

- Available: <https://www.sciencedirect.com/science/article/pii/S1359646219301150>
- [4] Z. L. Tseng, L. C. Chen, C. H. Chiang, S. H. Chang, C. C. Chen, C. G. Wu, *Efficient inverted-type perovskite solar cells using UV-ozone treated MoO<sub>x</sub> and WO<sub>x</sub> as hole transporting layers*. Sol. Energy 139 (2016, Winter) 484–8.  
Available: <https://www.sciencedirect.com/science/article/abs/pii/S0038092X16304698>
- [5] W. Chen, F. Z. Liu, X. Y. Feng, B. D. Aleksandra, K. C. Wai, Z. B. He, *Cesium doped NiO<sub>x</sub> as an efficient hole extraction layer for inverted planar perovskite solar cells*. Adv. Energy Mater. 7 (2017, Summer) 1700722.  
Available: <https://onlinelibrary.wiley.com/doi/10.1002/aenm.201700722>
- [6] S. Abdelaziz, A. Zekry, A. Shaker, M. Abouelatta, *Investigation the performance of formamidinium tin-based perovskite solar cell by SCAPS device simulation*, Opt. Mater. 101 (2020, Spring) 109738.  
Available: <https://www.sciencedirect.com/science/article/abs/pii/S0925346720300896>
- [7] M. S. Chowdhury, S. A. Shahahmadi, P. Chelavanathan, S. K. Tiong, N. Amin, K. Techato, N. Nuthammachot, T. Chowdhury, M. Suklueng, *Effect of deep-level defect density of the absorber layer and n/i interface in perovskite solar cell by SCAPS-1D*, Results Phys. 16 (2020, Spring) 102839.  
Available: <https://www.sciencedirect.com/science/article/pii/S2211379719321217>
- [8] A. Mirkamali, K.K. Muminov, *Numerical simulation of CdS/CIGS tandem multi-junction solar cells with AMPS-1D*, JOPN. 2(1) (2017, Winter) 31-40.  
Available: [http://jopn.miau.ac.ir/article\\_2198.html](http://jopn.miau.ac.ir/article_2198.html)
- [9] A. Hima, *GPVDM simulation of layer thickness effect on power conversion efficiency of CH<sub>3</sub>NH<sub>3</sub>PbI<sub>3</sub> based planar heterojunction solar cell*, IJECA. 3 (1) (2018) 37–41.  
Available: <https://www.ijeca.info/index.php/IJECA/article/view/64>
- [10] I. Silvaco, Atlas User's Manual, (2016).  
Available: <https://dynamic.silvaco.com/dynamicweb/jsp/downloads/DownloadManualsAction.do?req=silen-manuals&nm=atlas>
- [11] K. Tan, P. Lin, G. Wang, Y. Liu, Z. Xu, Y. Lin, *Controllable design of solid-state perovskite solar cells by SCAPS device simulation*. Solid State Electron. 126 (2016, Winter) 75-80.

Available: <https://www.sciencedirect.com/science/article/abs/pii/S0038110116301423>

- [12] G. A. Casas, M.A. Cappelletti, A. P. Cédola, B.M. Soucase, E. P. Blancá, *Analysis of the power conversion efficiency of perovskite solar cells with different materials as Hole-Transport Layer by numerical simulations*. Super lattice. Microst. 107 (2017, Summer) 136-143.

Available: <https://www.sciencedirect.com/science/article/abs/pii/S0749603617303087>

- [13] D. Ompong, J. Singh, *Charge carrier mobility dependent open-circuit voltage in organic and hybrid solar cells*, Front. Nanosci. Nanotech. 2(1) (2015) 43-47.

Available: <https://www.oatext.com/pdf/FNN-2-108.pdf>

